Materials Chemistry and Physics 138 (2013) 5–10

Contents lists available at SciVerse ScienceDirect

Materials Chemistry and Physics

journal homepage: www.elsevier.com/locate/matchemphys

Materials science communication

Fabrication of vertically aligned $CuInSe_2$ nanorod arrays by template-assisted mechanical approach

Manisha Kondiba Date [a,b], Bo-Cheng Chiu [c], Chin-Hung Liu [a,b], Yu-Ze Chen [a,b], Yi-Chung Wang [a,b], Hsing-Yu Tuan [c], Yu-Lun Chueh [a,b,*]

[a] Department of Materials Science and Engineering, National Tsing Hua University, Hsinchu 300, Taiwan, ROC
[b] Center For Nanotechnology, Material Science, and Microsystem, National Tsing Hua University, No. 101, Sec. 2, Kuang-Fu Rd., Hsinchu 30013, Taiwan, ROC
[c] Department of Chemical Engineering, National Tsing Hua University, Hsinchu 300, Taiwan, ROC

HIGHLIGHTS

- Aligned NR arrays were fabricated from NPs by template-assisted mechanical approach.
- Large scale nanostructures with superior optical properties were achieved.
- Polycrystalline NRs with $CuInSe_2$ tetragonal phase were obtained.

ARTICLE INFO

Article history:
Received 26 March 2012
Received in revised form
25 October 2012
Accepted 18 November 2012

Keywords:
Semiconductors
Crystal growth
Optical properties
Electron microscopy (STEM, TEM and SEM)
Heat treatment

ABSTRACT

A facile, low cost, and vacuum free method for fabricating vertically aligned copper indium diselenide ($CuInSe_2$) nanorod (NR) arrays from pre-synthesized $CuInSe_2$ nanoparticles (NPs) by mechanical approach using porous anodic aluminum oxide (AAO) as a template was demonstrated. This approach utilizes a rubbing technique to fill $CuInSe_2$ NPs suspension into AAO template. X-ray diffraction and Raman spectroscopy study is employed to confirm the phase of $CuInSe_2$ NPs before and after the formation of NRs. The polycrystallinity and composition of NRs are confirmed by using transmission electron microscopy. Optical studies of $CuInSe_2$ NPs film reveal a reflectance of ~9.8% while a significant reduction of the reflectance to ~1.2% is observed after the formation of $CuInSe_2$ NR arrays. The observed low reflectance behavior is attributed to a concept of gradual refractive index with vertical array structures. From differential reflectance spectra of $CuInSe_2$ NRs, a band gap of ~1.01 eV was observed, which is identical to its bulk value.

1. Introduction

Limited natural fuel resources, environmental issues, and growing demand for energy compelled the researchers and policy makers to search for alternative renewable and clean energy sources [1]. Thus, searching for alternative renewable and clean energy has become an urgent demand, which has recently attracted enormous attention of the scientists worldwide. Among the plethora of alternative renewable energy being explored, solar energy is considered as one of the most promising candidates; while developing efficient solar cells has become a potential challenge for converting solar energy into electrical energy to satisfy the growing demand [2]. Silicon-based leading materials, including single and polycrystalline structures have been extensively studied [3,4]. However, required purity, emission of CO_2 during processing, high processing cost, etc. are some drawbacks of silicon-based solar cells and the indirect band gap limits the efficiency of Si-based solar cells [5]. Among all solar cell materials for photovoltaic (PV) applications, chalcopyrite semiconductors are the most promising light absorbing materials [6] and are considered as a better alternative to silicon-based materials. The compounds of I–III–IV_2 group elements have attracted much attention in recent years because of their unique electronic and optical properties that make them suitable to achieve better energy conversion [7]. Among them, $CuInSe_2$ (CIS)-based thin film solar cells are a promising type of the renewable PV [8], which has an advantage of thinner absorber layer below the thickness of 2 μm [9]. Furthermore, due to its direct band gap, low cost, high absorption coefficient, good radiation stability, long term optoelectronic stability, and unique structure, it is considered to be a promising material [10–16]. Earlier reports have shown that thin film CIS solar cells have

* Corresponding author. Department of Materials Science and Engineering, National Tsing Hua University, Hsinchu 300, Taiwan, ROC.
E-mail address: ylchueh@mx.nthu.edu.tw (Y.-L. Chueh).

0254-0584/$ – see front matter © 2012 Elsevier B.V. All rights reserved.
http://dx.doi.org/10.1016/j.matchemphys.2012.11.047

exhibited the highest efficiency of ~20%, which is higher than those of single crystalline silicon solar cells [8]. Fabrication of nanostructured $CuInSe_2$ thin films by physical deposition methods require stringent conditions like high temperature, high vacuum system, skilled personnel, etc. which leads to higher production cost. To circumvent these problems, development of a new low cost, easily scalable, high throughput method without the use of high vacuum process is imperative [17,18].

One-dimensional nanowire-based nanostructures provide better efficient charge collection due to their radial junction structure and cylindrical geometry whereas the anti-reflectivity of nanostructure enhances light trapping and absorption [19–21]. In the past decade, many techniques have been developed to create different nanostructure arrays for solar cell device, including growth of II–VI semiconductor nanopillar arrays from highly periodic anodic aluminum membranes (AAMs), epitaxial growth of nanowire arrays from lattice matched substrate, and chemical/physical etching or deposition on patterned substrate [22–24]. However, they are limited by the impracticality for mass production over large area.

With this regard, we demonstrate a fabrication of vertically aligned $CuInSe_2$ NR arrays by a simple, non-vacuum, template-assisted mechanical approach. Compared to high vacuum methods, this method is cost effective and provides nanostructures with controlled dimensions. Morphological study of the $CuInSe_2$ nanorods (NRs) was accomplished by scanning electron microscopy (SEM) and transmission electron microscopy (TEM). To observe the cross section view of whole NRs, focused ion beam (FIB) cutting was used to cut the sample and then analyzed by SEM. X-ray diffraction (XRD) pattern and selected area electron diffraction (SAED) pattern examinations of the $CuInSe_2$ NRs were used to confirm the crystalline structure. Composition analysis was performed using energy dispersive spectroscopy (EDS) attached to a TEM. Phase confirmation of NPs and NR array was analyzed by Raman spectroscopy, whereas the optical measurements were carried out by UV–Vis spectroscopy.

2. Experimental section

2.1. Preparation of anodic aluminum oxide template

For preparation of anodic aluminum oxide template, a two-step anodization process was used [25,26]. An aluminum sheet with thickness of 200 μm (Alfa Aesar, purity 99.999%, molecular weight (MW): 26.98 g mol^{-1}) was used as a starting material and it acted as an anode, while the carbon acted as a counter-electrode. A solution containing 0.1 M oxalic acid (Sigma Aldrich, purity >99.5%, molecular weight (MW): 126.7 g mol^{-1}) was used as an electrolyte. First-step anodization was accomplished under a constant voltage of 160 V for 1 h at 1 °C. Alumina formed in the first anodization step was etched-off by immersing sample in a mixed acid solution of phosphoric acid (Sigma Aldrich, purity >95%, molecular weight (MW): 98 g mol^{-1}) and chromic acid (Sigma Aldrich, purity ≥99.8%, molecular weight (MW): 118 g mol^{-1}) solution (6 wt.% H_3PO_4 + 1.8 wt.% H_2CrO_4) at 60 °C. The Second-step anodization process was carried out at the constant voltage of 160 V at room temperature for 3 h, yielding porous aluminum oxide layer.

2.2. Synthesis of $CuInSe_2$ NPs via heating-up method

The reactants used in present study are 12 mL oleylamine (OLA) (Sigma Aldrich, purity 70%, molecular weight (MW): 267.49 g mol^{-1}), 0.5 mM CuCl (Alfa Aesar, purity 99.999%, molecular weight (MW): 98.99 g mol^{-1}), 0.5 mM $InCl_3$ (Sigma Aldrich, purity 99.999%, molecular weight (MW): 221.18 g mol^{-1}) and 1 mM elemental Se (Sigma Aldrich, purity 99.99%, molecular weight (MW): 78.96 g mol^{-1}). Cu, In, and Se precursors with ratio of 1:1:2 were used with OLA in a three neck flask, which was connected to condenser, Schlenk line, and thermocouple while one neck was sealed. Temperature was maintained at 130 °C in presence of argon and flask was purged with oxygen for 1 h with continuous stirring of reaction mixture. The temperature was gradually increased with a rate of 2.3 °C min^{-1} until a final temperature of 265 °C was achieved and the reaction was allowed to continue for 1.5 h with a constant stirring. Thereafter, the flask was cooled down to room temperature and the NPs were precipitated by adding ethanol (Sigma Aldrich, purity 99.8%, Molecular weight (MW): 46.07 g mol^{-1}) and separated by centrifugation for 10 min. Finally, the NPs were re-dispersed in toluene solution (JT Baker, purity ≥99.5%, molecular weight (MW): 92.14 g mol^{-1}) [17]. $CuInSe_2$ NP film was prepared by spin coating of as synthesized NP suspension and used for UV–vis–NIR measurements, XRD and Raman analysis.

2.3. Fabrication of $CuInSe_2$ NRs via template-assisted mechanical approach

A schematic illustration of template-assisted mechanical approach is shown in Fig. 1. The AAO template was first pretreated by O_2 plasma for 3 min at 200 W with an oxygen gas flow of 100 sccm in order to increase hydrophilicity on surface of the AAO template as shown in Fig. 1(a). A drop of 5 μL $CuInSe_2$ NPs solution dispersed in toluene (25 mg mL^{-1}) was drop-cast on the pretreated AAO surface [17]. A sheet of PDMS (Dow Corning, Sylgard 184A and Sylgard 184B with ratio of 1:10) with a thickness of ~2.5 mm was used for template-assisted mechanical approach, with which the NPs solution drop-cast on AAO was rubbed on the surface along the direction parallel to AAO surface (Fig. 1(b)). With the rubbing motion, force was applied on PDMS sheet to drive the NPs suspension inside the AAO nanopores (Fig. S1 in Supplementary material). It is important to note that, since PDMS is inert [27], no chemical reaction occurred with the NP solution. The rubbing process was repeated to ensure the filling of $CuInSe_2$ NPs suspension inside AAO template and the formation of $CuInSe_2$ NR arrays as shown in Fig. 1(c). During the rubbing process, several drops of NPs solution with each drop of 5 μL volume, were used for filling of the AAO and further checked by SEM images. To completely fill the selected dimensions of the AAO, about 80 drops with each drop of

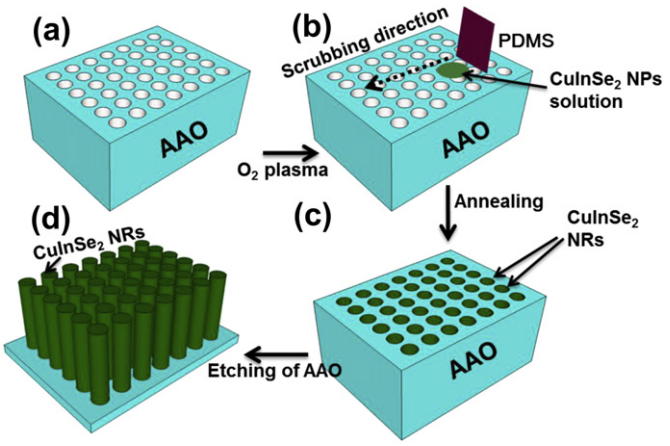

Fig. 1. Schematic illustration of the fabrication of nanorods by template-assisted mechanical approach: (a) empty AAO, (b) mechanical filling of NPs suspension inside AAO pores using PDMS sheet, (c) NRs inside AAO after thermal annealing and (d) Vertically aligned NR arrays after removal of AAO in NaOH solution.

5 μL $CuInSe_2$ NPs solution, were used for continuous rubbing process. Subsequently, in order to remove the residual solvent, the samples were annealed for 3 h in vacuum at 250 °C in presence of argon gas at 50 sccm. Consequently, vertically aligned $CuInSe_2$ NR arrays within the AAO template were obtained. The AAO template with vertically aligned $CuInSe_2$ NR arrays was further treated with 0.1 M sodium hydroxide (NaOH) solution for 3 min to remove AAO as shown in Fig. 1(d).

2.4. Process of removing AAO template

In order to observe vertically aligned NR arrays by SEM, the sample was prepared for etching of AAO. An epoxy layer was deposited on glass substrate and the upper surface of NPs filled AAO (upside down) was sticked to the epoxy layer. In the first step, the prepared sample was etched by 0.3 M copper chloride solution (Showa, purity 98%, molecular weight (MW): 134.45 g mol^{-1}) prepared in hydrochloric acid solution (Sigma Aldrich, purity 36%, molecular weight (MW): 36.46 g mol^{-1}) until aluminum layer was completely removed. Sample was immediately washed with isopropyl alcohol and deionized water. Subsequently, the sample was etched in 0.1 M sodium hydroxide (NaOH) solution (JT Baker, molecular weight (MW): 40 g mol^{-1}) for 20 s, washed with deionized water and dried with nitrogen purging. The sample was then analyzed by SEM to ensure the etching of AAO. Since the sample was not etched completely, it was again etched in 0.1 M NaOH solution for 10 s (total etching time: 30 s), followed by washing, drying and morphology analysis by SEM. Until the AAO was removed completely, the sample from the above step was successively etched by 0.1 M NaOH for total etching time of 1 min and 3 min. It was observed that at the total etching time of 3 min, complete removal of AAO takes place to obtain free-standing vertically aligned NR array. Further analysis was done by SEM, XRD, UV–vis, and Raman. For cross-sectional TEM sample preparation of NRs, a SiO_2 layer with a thickness of ~300 nm was deposited by E-gun on the top surface of NRs embedded in AAO.

2.5. Characterization

Morphologies and microstructures of $CuInSe_2$ NRs in AAO and NRs after removal of AAO were studied by field-emission scanning electron microscopy (FE-SEM, JSM-6500F, JEOL) operated at 15 kV. To observe the cross sectional view of SEM image for whole NRs, the sample was prepared by focused ion beam (FIB, Hillsbore, FEI Nova 200) operated at 25 kV with Ga ion source. Crystal structure of $CuInSe_2$ NR arrays sample after removal of the AAO template was characterized by X-ray diffractometer (XRD, SHIMADZU, 6000) operated with scan ranges of 20°–80° at 20 mA, 30 kV, step size of 0.02, a scan rate of 2°/min and 30 min time per step. Crystal structure of the $CuInSe_2$ NP film and NR arrays in the AAO template was characterized by Grazing Incident Angle X-ray diffractometer (GIAXRD, MAC Science, MX P18) with Cu $K\alpha_1$ ($\lambda = 0.154$ nm) as the radiation source. GIAXRD diffraction data was collected with two-theta angle ranging from 20° to 80° at 150 mA, 40 kV, step size of 0.02, a scan rate of 4°/min and 15 min time per step. Low resolution bright field transmission electron microscopy (TEM) images were taken by JEOL JEM-3000F at accelerating voltage of 300 keV. Composition of $CuInSe_2$ NRs was

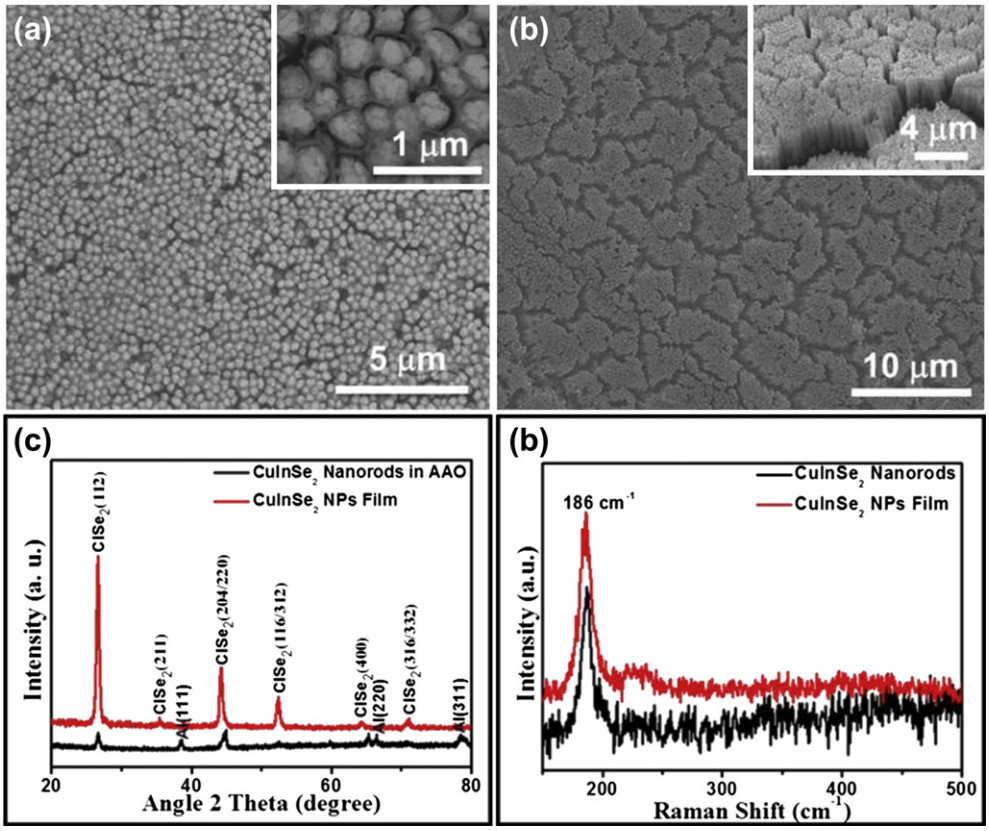

Fig. 2. (a) Top view SEM image of $CuInSe_2$ NRs in AAO pores. Inset: enlarged SEM image of NRs in AAO pores, indicating the complete filling of AAO. (b) Top view SEM image of vertically aligned NR array after removal of AAO. Inset: SEM image of NR arrays with titling angle of 30°. (c) XRD spectra of $CuInSe_2$ NPs film on glass substrate and $CuInSe_2$ NRs in AAO template. (d) Raman spectra of $CuInSe_2$ NPs film and $CuInSe_2$ NRs after removal of AAO [JCPDS card no: 40-1487 for $CuInSe_2$ phase and JCPDS card no: 85-1327 for aluminum phase].

determined with an energy dispersive spectrometer (EDS) attached to the TEM. Phase analysis of NRs and NP film was achieved by Raman spectroscopy using HORIBA, HR 800UV. UV–vis–NIR transmittance and reflectance spectra were obtained with a HITACHI UV-4100 spectrophotometer at resolution of 5 nm, slit width of 4 nm, path length of 10 mm, and scan speed of 2400 nm min^{-1}. For optical study, spin coated film of as synthesized NPs on the glass substrate as well as fabricated NRs placed on the glass/epoxy substrate after removal of AAO template was used.

3. Results and discussion

Porous aluminum oxide layer with thickness and pore diameters of ~1.4–1.5 μm and 250–300 nm was prepared, respectively and used as a template for fabrication of NR arrays. Fig. 2(a) shows a top view SEM image after suspension filling of $CuInSe_2$ NPs inside the AAO pores via the mechanical approach followed by thermal annealing. The inset shows the enlarged SEM image of $CuInSe_2$ NRs with an average diameter of ~300 nm. For a typical AAO template with a porosity of ~25% [28], more than 99% of pores were filled with NPs, providing a significant evidence of fast and high throughput process based on this mechanical approach. The top aluminum oxide layer was removed by copper chloride solution (see Experimental section for more details) and the AAO template was then etched in 0.1 M NaOH solution for different etching time (Fig. S2a–d in Supplementary material). After etching AAO for 20 s, transparent hemispherical AAO appears on the surface (Fig. S2a in Supplementary material). After etching AAO for 30 s, a few opened hemispheres from one side were observed (Fig. S2b in Supplementary material). Almost 30% of AAO was removed after 1 min of etching time (Fig. S2c in Supplementary material) while a complete removal of AAO template was achieved after an etching time of 3 min (Fig. S2d in Supplementary material). A representative SEM image after complete removal of AAO is shown in Fig. 2(b), which shows free-standing vertically aligned NR array over large scale. Inset of Fig. 2(b) shows the enlarged SEM image with a tilting angle of 30°. Fig. 2(c) shows XRD spectra of $CuInSe_2$ NPs film and NRs embedded in the AAO template. Characteristic peaks at 26.57, 35.43, 44.19, 52.43, 64.40 and 71.05 for $CuInSe_2$ NPs were indexed to be chalcopyrite structure from JCPDS data base (no: 40-1487), corresponding to the plane spacing of (112), (211), (204/220), (116/312), (400), and (316/332), respectively. XRD spectra of $CuInSe_2$ NRs in AAO show the same trend with peaks at 26.66, 44.64, and 52.52, corresponding to planes of (112), (204/220), and (116/312), were indexed, respectively. XRD spectra indicate that the formation of a pure tetragonal chalcopyrite structure for $CuInSe_2$ NRs is stable and is identical to bulk $CuInSe_2$ [29]. No impurity phases, such as Cu_xSe (JCPDS card no: 24-1131 (for Cu_2Se) and 6-0427 (for CuSe)), CuO (JCPDS card no: 5-0661), and InSe (JCPDS card no: 42-0919) were found. In XRD spectrum of $CuInSe_2$ NRs before removal of the AAO template, some characteristic aluminum (Al) peaks (JCPDS card no: 85-1327), which comes from the AAO template, were observed at 38.56, 66.48 and 78.45 corresponding to the plane spacing of (111), (220) and (311), respectively. In addition, the phase of $CuInSe_2$ remains even after removal of the AAO template, which was confirmed from XRD spectrum (Fig. S3 in Supplementary material). XRD spectra of the $CuInSe_2$ NRs embedded in AAO (Fig. 2(c)) show more aluminum peaks whereas the $CuInSe_2$ NRs after etching of the AAO template (Fig. S3 in Supplementary material) shows only one peak with much weaker intensity, which comes from residual AAO left on the substrate below the $CuInSe_2$ NRs. An increasing background at small diffraction angles

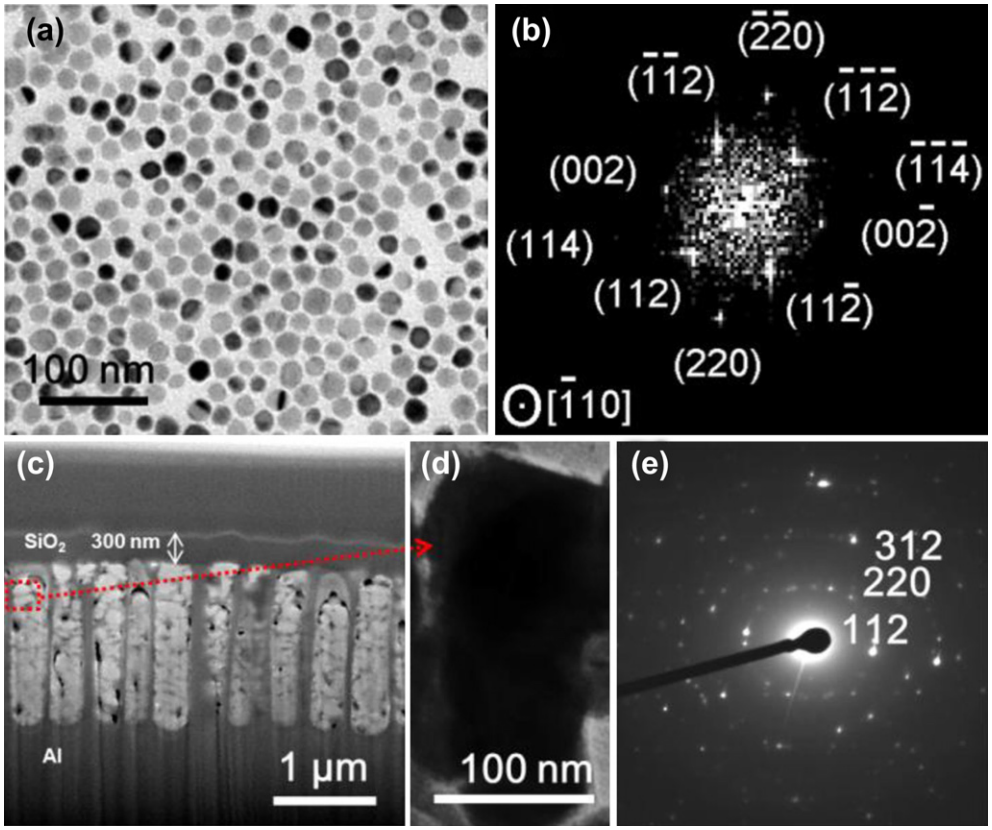

Fig. 3. (a) Low magnification TEM image of $CuInSe_2$ NPs. (b) The corresponding fast Fourier transform of $CuInSe_2$ NPs. (c) A cross section SEM image of NRs inside AAO nanopores prepared by FIB. (d) A TEM image of a part of $CuInSe_2$ NR. (e) Diffraction pattern of $CuInSe_2$ NR with preferred orientation planes.

can be found in the XRD pattern (Fig. S3 in Supplementary material), which may be induced by diffraction from the residual AAO or may be due to the amorphous epoxy layer on the substrate below the NRs. Raman spectra were used to further confirm the phase of the $CuInSe_2$ NRs as shown in Fig. 2(d). From previous Raman scattering studies of the chalcopyrite $CuInSe_2$, E(LO) mode is one of the Raman active mode, which has been reported in the frequency range of 182–184 cm^{-1}. However, it has been detected only in Raman analysis on (100)-oriented bulk single crystals at low temperature [30]. From Raman spectra analysis, the peak observed at 186 cm^{-1} (Fig. 2(d)), is close to the reported value of the chalcopyrite $CuInSe_2$ Raman active mode. For $CuInSe_2$ NP film as well as the NRs obtained after etching of the AAO structure shows an active peak at the same value, indicating no phase change occurred during the preparation of NRs from NPs.

To shed light on crystallinity of the $CuInSe_2$ NPs and NRs, transmission electron microscopy (TEM) observation is imperative. As shown in Fig. 3(a), a TEM image of NPs indicates that the diameter of NPs ranges from 10 to 25 nm and Fig. 3(b) shows a corresponding fast Fourier transform (FFT) with zone axis of [110]. The SEM image of sample after the sample prepared by focused ion beam (FIB) technique is shown in Fig. 3(c). Some voids were observed in NRs (Fig. 3(c)), which may be attributed to the FIB induced surface and sidewall damage. FIB induced damage was reported to be material dependent [31], whereas characterization done by Rubanov and Munroe demonstrated the surface- and sidewall damage for different materials with Ga^+ ion beams and found that the surface damage varied widely in thickness [32]. The previous reported syntheses of CIS and binary selenide have not achieved large grains after selenization process [33,34]. However, Guo et al. reported that after the sintering process, NPs can form larger grains [35]. Here, we expect that, the grains would be larger after annealing because the grain boundaries are the accumulation of point defects [36]. Importantly, length and diameter of the NRs were same as that of AAO, indicating that the dimensions of NRs could be controllable based on the dimensions of AAO. A TEM image taken from a part of Fig. 3(c) as shown in Fig. 3(d), reveals the polycrystalline feature owing to the recrystallization process from the NPs to NRs during thermal annealing, which is an interesting morphological feature of highly efficient solar cells.

A selected area electron diffraction (SAED) pattern of a NR in Fig. 3(e) reveals the ring-like pattern, confirming a polycrystalline nature of $CuInSe_2$ phase, where the (112), (220), and (312) planes can be indexed, respectively [37]. Atomic percentages of Cu, In, and Se measured from energy dispersive X-ray analysis (EDS) for $CuInSe_2$ NRs were found to be ~23.4, ~27.2, and ~50.4 at%, respectively, corresponding to atomic ratio of ~1:1:2 for Cu:In:Se and is in agreement with the $CuInSe_2$ NPs with atomic percentages of Cu, In, and Se to be ~24.3, ~25.2, and ~51.5 at%, respectively (Table 1). EDS spectra of $CuInSe_2$ NRs showed one intense peak, corresponding to Ni (Fig. S4 in Supplementary material), which comes from Ni grid during TEM analyses.

Nanostructures possess a refractive index matching with air that significantly suppresses light reflection over the whole spectrum as compared to thin film structure. The reflectance measurements of the $CuInSe_2$ NPs film and NRs are shown in Fig. 4(a). The $CuInSe_2$ NPs film shows the reflectance of ~9.8% while a significant reduction of reflectance to ~1.2% is achieved after the formation of

Table 1
Compositions of Cu, In, and Se for $CuInSe_2$ NPs and NR from EDS analysis.

	Cu (at%)	In (at%)	Se (at%)
$CuInSe_2$ NPs	24.3	25.2	51.5
$CuInSe_2$ NR	23.4	27.2	50.4

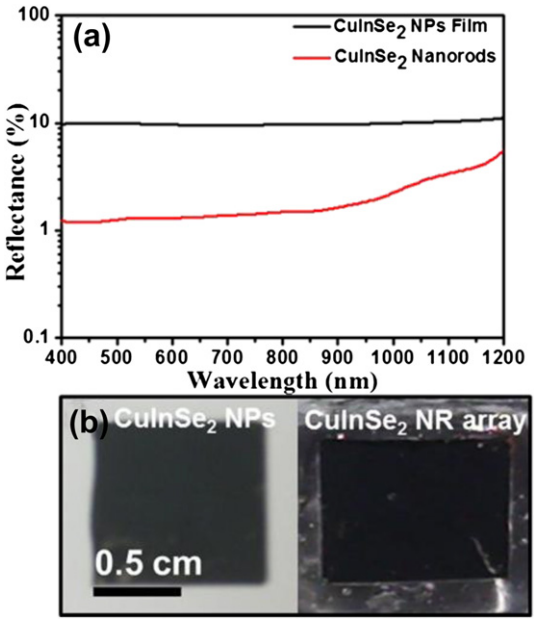

Fig. 4. (a) Reflectance spectra of $CuInSe_2$ NPs film and NR arrays after removal of AAO. (b) Optical images of samples for $CuInSe_2$ NPs film and NR arrays after removal of AAO.

NRs (Fig. 4(a)). The observed low reflectance behavior is attributed to a concept of gradual refractive index with vertical array structures. Therefore, the large Fresnel reflection on the planar $CuInSe_2$ surface is due to the refractive index mismatch between the air ($n = 1$) and $CuInSe_2$ ($n = 2.5$–3.8), which can be significantly reduced through a smooth transition of refractive index from the

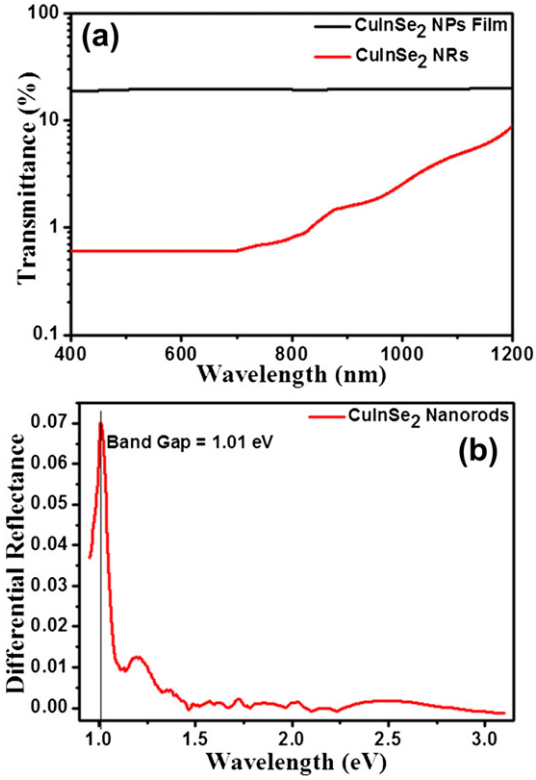

Fig. 5. (a) Transmittance spectra of $CuInSe_2$ NPs film and NR arrays after removal of AAO. (b) Differential reflectance spectra of $CuInSe_2$ NR arrays after removal of AAO (Band gap obtained is 1.01 eV.).

top to the base of the vertical $CuInSe_2$ NR arrays film [38]. Optical image as shown in Fig. 4(b) reveals the darkest color for the $CuInSe_2$ NRs in contrast to the $CuInSe_2$ NPs film. This remarkably low reflectance of the $CuInSe_2$ NRs film can be attributed to the vertical $CuInSe_2$ NRs with high density [39]. The $CuInSe_2$ NPs film shows a transmittance of ~19%, while a transmittance of ~0.6% is achieved after formation of NRs. (Fig. 5(a)). A very low transmittance was observed from the $CuInSe_2$ NRs film in the range of wavelengths from 400 to 700 nm, indicating that ~99% of light is absorbed by the $CuInSe_2$ NRs film. In addition, the band gap extracted from optical measurements 1.01 eV (Fig. 5(b)) is in good agreement with the reported value [16].

4. Conclusions

A simple, cost effective and vacuum free method is developed for the fabrication of vertically aligned $CuInSe_2$ NR array. SEM clearly shows AAO filled with $CuInSe_2$ NPs resulting in the formation of NRs inside AAO nanopores by mechanical rubbing technique. Length and diameter of the NRs were determined by that of AAO, indicating that the dimensions of NRs could be precisely controlled by controlling the dimensions of AAO. A pure tetragonal chalcopyrite phase of $CuInSe_2$ NRs was achieved with the composition of NRs nearly equal to $CuInSe_2$ NPs composition. No phase change was observed even after the formation of NRs from NPs, whereas, SAED pattern analysis confirmed polycrystalline nature of $CuInSe_2$ NRs. Optical properties of the $CuInSe_2$ NRs compared to that of NPs film show that the $CuInSe_2$ NRs structure demonstrate better optical performance than NP film. This template-assisted mechanical approach for the fabrication of vertically aligned NR arrays is simple and inexpensive; also it could be extended to other NPs for synthesis of vertically aligned nanostructure arrays for different applications. By applying the NPs with different band gaps in one NR, a concept of vertically tandem NR arrays with high density can be feasibly achieved, which can be adapted for large area production and reduction of cost. We believe that the further development of this potential approach could be useful for industrialization of low cost nanostructure solar cells.

Acknowledgments

This research was supported by the National Science Council through Grant No. 101-2622-E-007-011-CC2, NSC 101-2218-E-007-009-MY3, and National Tsing Hua University through Grant No. 100N2024E1. Y.L. Chueh greatly appreciates the use of facility at CNMM the National Tsing Hua University through Grant No. 101N2744E1.

Appendix A. Supplementary material

Supplementary material associated with this article can be found in the online version, at http://dx.doi.org/10.1016/j.matchemphys.2012.11.047.

References

[1] V.S. Arunachalam, E.L. Fleischer, MRS Bull. 33 (2008) 261.
[2] M.S. Dresselhaus, I.L. Thomas, Nature 414 (2001) 332–337.
[3] P. Wurfel, Physics of Solar Cells, From Principles to New Concepts, Wiley-VCH, Weinheim, 2005.
[4] K. Yamamoto, M. Yoshimi, T. Suzuki, Y. Tawada, Y. Okamoto, A. Nakajima, S. Igari, in: Proc. 2nd World Conf. on PV Solar Energy Conversion, 1998. pp. 1284.
[5] M. Kirkengen, J. Bergli, Y.M. Galperin, J. Appl. Phys. 102 (2007) 093713-1–093713-5.
[6] Maziar Afshar, Sascha Sadewasser, Jürgen Albert, Sebastian Lehmann, Daniel Abou-Ras, David Fuertes Marrón, Angus A. Rockett, Esa Räsänen, Martha Ch. Lux-Steiner, Adv. Energy Mater. 1 (2011) 1109–1115.
[7] C. Tablero, Thin Solid Films 519 (2010) 1435–1440.
[8] I. Repins, M.A. Contreras, B. Egaas, C. DeHart, J. Scharf, C.L. Perkins, B. To, R. Noufi, Prog. Photovoltaics Res. Appl. 16 (2008) 235–239.
[9] CIS Photovoltaic Module, EU/ASIA-PACIFIC Edition, Solar Frontier, Source: New Energy and Industrial Technology Development Organization (NEDO).
[10] D. Cahen, J.M. Gilet, C. Schmitz, L. Chernya, K. Gartsman, A. Jakubowicz, Science 258 (1992) 271–274.
[11] A.A.I. Al-Bassam, Mater. Chem. Phys. 53 (1998) 1–5.
[12] R. Inguanta, L. Patrizia, P. Salvatore, S. Carmelo, Electrochem. Solid-State Lett. 13 (2010) K22–K25.
[13] K. Ramanathan, M.A. Contreras, C.L. Perkins, S. Asher, F.S. Hasoon, J. Keane, D. Young, M. Romero, W. Metzger, R. Noufi, J. Ward, A. Duda, Prog. Photovoltaics Res. Appl. 11 (2003) 225–230.
[14] J.F. Guillemoles, U. Rau, L. Kronik, H.W. Schock, D. Cahen, Adv. Mater. 11 (1999) 957–961.
[15] Y.H. Yang, Y.T. Chen, J. Phys. Chem. B 110 (2006) 17370–17374.
[16] C. Guillén, J. Herrero, Sol. Energy Mater. Sol. Cells 72 (2002) 141–149.
[17] M.Y. Chiang, S.H. Chang, C.Y. Chen, F.W. Yuan, H.Y. Tuan, J. Phys. Chem. C 115 (2011) 1592–1599.
[18] L.Y. Zhu, X.Q. Wang, Q. Ren, G.H. Zhang, D. Xu, Mater. Chem. Phys. 133 (2012) 445–451.
[19] R.S. Devan, R.A. Patil, J.H. Lin, Y.R. Ma, Adv. Funct. Mater. 22 (2012) 3326–3370.
[20] X.D. Li, D.W. Zhang, S. Chen, Z.A. Wang, Z. Sun, X.J. Yin, S.M. Huang, Mater. Chem. Phys. 124 (2010) 179–183.
[21] L. Zhang, J. Liang, S. Peng, Y. Shi, J. Chen, Mater. Chem. Phys. 106 (2007) 296–300.
[22] E.A. Hernández-Pagán, W. Wang, T.E. Mallouk, ACS Nano 5 (2011) 3237–3241.
[23] J. Zhu, C.M. Hsu, Z.F. Yu, S.H. Fan, Y. Cui, Nano Lett. 10 (2010) 1979–1984.
[24] W.I. Park, Appl. Phys. Lett. 80 (2002) 4232–4234.
[25] H. Masuda, H. Yamada, M. Satoh, H. Asoh, M. Nakao, T. Tamamura, Appl. Phys. Lett. 71 (1997) 2770–2772.
[26] F.Y. Li, L. Zhang, R.M. Metzger, Chem. Mater. 10 (1998) 2470–2480.
[27] J.F. Künzler, Trends Polym. Sci. 4 (1996) 52–59.
[28] P. Liu, V.P. Singh, S. Rajaputra, S. Phok, Z. Chen, J. Mater. Res. 25 (2010) 207–212.
[29] C.C. Wu, C.Y. Shiau, D.W. Ayele, W.N. Su, M.Y. Cheng, C.Y. Chiu, B.J. Hwang, Chem. Mater. 22 (2010) 4185–4190.
[30] H. Tanino, T. Maeda, H. Fujikake, H. Nakanishi, S. Endo, T. Irie, Phys. Rev. B 45 (1992) 13323–13330.
[31] M.W. Phaneuf, Micron 30 (1999) 277–288.
[32] S. Rubanov, P.R. Munroe, Microsc. Microanal 11 (2005) 446–455.
[33] C. Eberspacher, C. Fredric, K. Pauls, J. Serra, Thin Solid Films 387 (2001) 18–22.
[34] M. Kaelin, D. Rudmann, F. Kurdesau, T. Meyer, H. Zogg, A.N. Tiwari, Thin Solid Films 431–432 (2003) 58–62.
[35] Q. Guo, S.J. Kim, M. Kar, W.N. Shafarman, R.W. Birkmire, E. A Stach, R. Agrawal, H.W. Hillhouse, Nano Lett. 8 (2008) 2982–2987.
[36] F.J. Humphreys, M. Haterly, Recrystallization and Related Annealing Phenonmena, second ed., Elsevier, 2004, pp. 150.
[37] H. Chen, S.M. Yu, D.W. Shin, J.B. Yoo, Nanoscale Res. Lett. 5 (2010) 217–223.
[38] S. Prabahar, V. Balasubramanian, N. Suryanarayanan, N. Muthukumarasamy, Chalcogenide Lett. 7 (2010) 49–58.
[39] T.H. Pei, S. Thiyagu, Z. Pei, Appl. Phys. Lett. 99 (2011) 153108–153111.